

Control Barrier Functions in UGVs for Kinematic Obstacle Avoidance: A Collision Cone Approach

Phani Thontepu^{*1}, Bhavya Giri Goswami^{*1}, Neelaksh Singh¹, Shyamsundar P I¹, Shyam Sundar M G¹, Suresh Sundaram¹, Vaibhav Katewa¹, Shishir Kolathaya¹

Abstract— In this paper, we propose a new class of Control Barrier Functions (CBFs) for Unmanned Ground Vehicles (UGVs) that help avoid collisions with kinematic (non-zero velocity) obstacles. While the current forms of CBFs have been successful in guaranteeing safety/collision avoidance with static obstacles, extensions for the dynamic case have seen limited success. Moreover, with the UGV models like the unicycle or the bicycle, applications of existing CBFs have been conservative in terms of control, i.e., steering/thrust control has not been possible under certain scenarios. Drawing inspiration from the classical use of collision cones for obstacle avoidance in trajectory planning, we introduce its novel CBF formulation with theoretical guarantees on safety for both the unicycle and bicycle models. The main idea is to ensure that the velocity of the obstacle w.r.t. the vehicle is always pointing away from the vehicle. Accordingly, we construct a constraint that ensures that the velocity vector always avoids a cone of vectors pointing at the vehicle. The efficacy of this new control methodology is experimentally verified on the Copernicus mobile robot. We further extend it to self-driving cars in the form of bicycle models and demonstrate collision avoidance under various scenarios in the CARLA simulator.

I. INTRODUCTION

Advances in autonomy have enabled robot application in all kinds of environments and in close interactions with humans, including autonomous navigation. Thus, designing controllers with formal safety guarantees have become an essential aspect of such safety-critical applications and an active research area in recent years. Researchers have developed many tools to handle this problem, such as model predictive control (MPC) [1], reference governor [2], reachability analysis [3] [4], artificial potential fields [5]. To obtain formal guarantees on safety (e.g., collision avoidance with obstacles), a safety critical control algorithm encompassing the trajectory tracking / planning algorithm is required that prioritizes safety over tracking. Control Barrier Functions [6] (CBFs) based approach is one such strategy in which a safe state set defined by inequality constraints is designed for the vehicle, and its quadratic programming (QP) formulation ensures forward invariance of these sets for all time.

A prime advantage of using CBF based quadratic programs is that they work efficiently on real-time practical applications; that is, optimal control inputs can be computed at a very high frequency on of-the-shelf electronics. It can be applied as a fast safety filter over existing path planning

This research was supported by the Wipro IISc Research Innovation Network (WIRIN).

¹Robert Bosch Center for Cyber Physical Systems (RBCCPS), Indian Institute of Science (IISc), Bengaluru. {vkatewa, shishirk}@iisc.ac.in

*These authors have contributed equally.

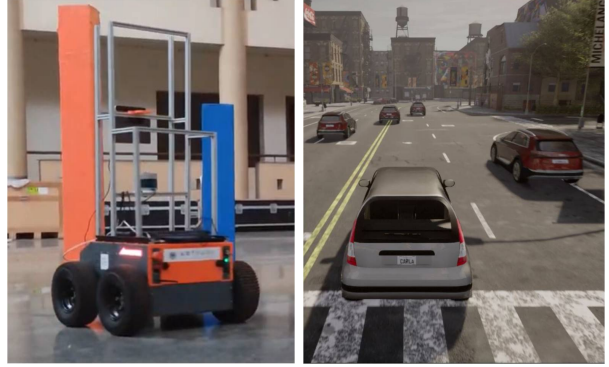


Fig. 1: Test setups: Copernicus UGV (left); Self driving vehicle in CARLA simulator (right).

controllers [7]. They are already being used for different behaviors in UGV's and self driving cars like Adaptive Cruise Control (ACC) [8], lane changing [9], obstacle avoidance [10] [11] [12] and roundabout crossings [13]. However, two major challenges remain that prevent successful deployment of these CBF-QPs in autonomous systems: a) Existing CBFs are not able to handle nonholonomic nature of autonomous vehicles well. They provide limited control capability in models like the unicycle and bicycle models i.e., the solutions from the CBF-QPs have either no steering or forward thrust capability under certain cases (this is shown in Section II), and b) Existing CBFs are not able to handle dynamic obstacles well i.e., the controllers are not able to avoid collisions with moving obstacles, which is also shown in Section II.

With the goal of addressing the above challenges, we propose a new class of CBFs via the collision cone approach. In particular, we generate a new class of constraints that ensure that the relative velocity between the obstacle and the vehicle always points away from the direction of vehicle's approach. Assuming ellipsoidal shape for the obstacles [14], the resulting set of unwanted directions for potential collision forms a conical shape, giving rise to the synthesis of **Collision Cone Control Barrier Functions (C3BFs)**. The C3BF based QP optimally calculates inputs such that the relative velocity vector direction is kept out of the collision cone (unsafe set) for all time. The approach is incorporated and demonstrated using the acceleration-controlled unicycle and bicycle models (see Fig. 1).

The idea of collision cones was first introduced in [14]–[16] as a means to geometrically represent the possible set

of velocity vectors of the vehicle that lead to collision. The approach was extended for irregular shaped robots and obstacles with unknown trajectories both in 2D [14] and 3D space [17]. This was commonly used for aerospace applications like missile guidance [18] and conflict detection and resolution in aircrafts [19]. This was further extended to Model Predictive Control by formulating the cones as constraints [20]. In our work, we combine the collision cone approach with CBFs to develop a novel obstacle avoiding algorithm for UGVs. With the benefits of both CBFs and Collision cone model, our C3BF algorithm is computationally efficient, works well in both static & dynamics environments, and guarantees safety. We will demonstrate this both in simulation and experiments.

Outline: Section II mathematically defines the CBF formulation. We also discuss different vehicle models used and their associated complexities. Section III begins with the intuition behind the approach of combining CBF and collision cones, followed by a detailed introduction to the formulation of C3BF. Section IV describes the simulations and experimental results obtained. Section V contains conclusions and future work on C3BF.

Notation: A continuous function $\kappa : [0, d] \rightarrow [0, \infty)$ for some $d > 0$ is said to belong to class- \mathcal{K} if it is strictly increasing and $\kappa(0) = 0$. Here, d is allowed to be ∞ . The same function can be extended to the interval $\kappa : (-b, d) \rightarrow (-\infty, \infty)$ with $b > 0$ (which is also allowed to be ∞), in which case we call it the extended class \mathcal{K} function. $\langle \cdot, \cdot \rangle$ denotes the inner product of two vectors.

II. BACKGROUND

In this section, we provide the relevant background necessary to formulate our problem of moving obstacle avoidance. Specifically, we first describe the vehicle models considered in our work; namely the unicycle and the bicycle models. Next, we formally introduce Control Barrier Functions (CBFs) and their importance for real-time safety-critical control for these types of vehicle models. Finally, we explain the shortcomings in existing CBF approaches in the context of collision avoidance of moving obstacles.

A. Vehicle models

1) *Acceleration controlled unicycle model:* A unicycle model has state variables $x_p, y_p, \theta, v, \omega$ denoting the pose, linear velocity, and angular velocity, respectively. The control inputs are linear acceleration (a) and angular acceleration (α). In Fig. 2 we show a differential drive robot, which is modeled as a unicycle. The resulting dynamics of this model is shown below:

$$\begin{bmatrix} \dot{x}_p \\ \dot{y}_p \\ \dot{\theta} \\ \dot{v} \\ \dot{\omega} \end{bmatrix} = \begin{bmatrix} v \cos \theta \\ v \sin \theta \\ \omega \\ 0 \\ 0 \end{bmatrix} + \begin{bmatrix} 0 & 0 \\ 0 & 0 \\ 0 & 0 \\ 1 & 0 \\ 0 & 1 \end{bmatrix} \begin{bmatrix} a \\ \alpha \end{bmatrix} \quad (1)$$

While the commonly used unicycle model in literature includes linear and angular velocities v, ω as inputs, we use

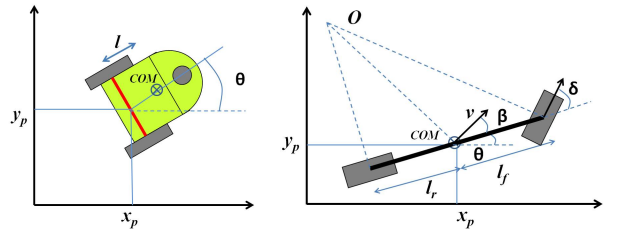


Fig. 2: Schematic of Unicycle (left); Bicycle model (right).

accelerations as inputs. This is due to the fact that differential drive robots have torques as inputs to the wheels that directly affect accelerations. In other words, we can treat the force / acceleration applied from the wheels as inputs. As a result, v, ω become state variables in our model.

2) *Acceleration controlled bicycle model:* The bicycle model has two wheels, where the front wheel is used for steering (see Fig. 2). This model is typically used for self-driving cars, where we treat the front and rear wheel sets as a single virtual wheel (for each set) by considering the difference of steer in right and left wheels to be negligible [9], [21], [22]. The bicycle dynamics is as follows:

$$\begin{bmatrix} \dot{x}_p \\ \dot{y}_p \\ \dot{\theta} \\ \dot{v} \end{bmatrix} = \begin{bmatrix} v \cos(\theta + \beta) \\ v \sin(\theta + \beta) \\ \frac{v}{l_r} \sin(\beta) \\ a \end{bmatrix}, \quad (2)$$

$$\text{where } \beta = \tan^{-1} \left(\frac{l_r}{l_f + l_r} \tan(\delta) \right), \quad (3)$$

x_p and y_p denote the coordinates of the vehicle's centre of mass (CoM) in an inertial frame. θ represents the orientation of the vehicle with respect to the x axis. a is linear acceleration at CoM. l_f and l_r are the distances of the front and rear axle from the CoM, respectively. δ is the steering angle of the vehicle and β is the vehicle's slip angle, i.e., the steering angle of the vehicle mapped to its CoM (see Fig. 2). This is not to be confused with the tire slip angle.

Remark 1: Similar to [9], we assume that the slip angle is constrained to be small. As a result, we approximate $\cos \beta \approx 1$ and $\sin \beta \approx \beta$. Accordingly, we get the following simplified dynamics of the bicycle model:

$$\begin{bmatrix} \dot{x}_p \\ \dot{y}_p \\ \dot{\theta} \\ \dot{v} \end{bmatrix} = \underbrace{\begin{bmatrix} v \cos \theta \\ v \sin \theta \\ 0 \\ 0 \end{bmatrix}}_{\dot{x}} + \underbrace{\begin{bmatrix} 0 & -v \sin \theta \\ 0 & v \cos \theta \\ 0 & \frac{v}{l_r} \\ 1 & 0 \end{bmatrix}}_{g(x)} \underbrace{\begin{bmatrix} a \\ \beta \end{bmatrix}}_u. \quad (4)$$

Since the control inputs a, β are now affine in the dynamics, CBF based Quadratic Programs (CBF-QPs) can be constructed directly to yield real-time control laws, as explained next.

B. Control barrier functions (CBFs)

Having described the vehicle models, we now formally introduce Control Barrier Functions (CBFs) and their applications in the context of safety. Consider a nonlinear control

system in affine form:

$$\dot{x} = f(x) + g(x)u \quad (5)$$

where $x \in \mathcal{D} \subseteq \mathbb{R}^n$ is the state of system, and $u \in \mathbb{U} \subseteq \mathbb{R}^m$ the input for the system. Assume that the functions $f : \mathbb{R}^n \rightarrow \mathbb{R}^n$ and $g : \mathbb{R}^n \rightarrow \mathbb{R}^{n \times m}$ are continuously differentiable. Given a Lipschitz continuous control law $u = k(x)$, the resulting closed loop system $\dot{x} = f_{cl}(x) = f(x) + g(x)k(x)$ yields a solution $x(t)$, with initial condition $x(0) = x_0$. Consider a set \mathcal{C} defined as the *super-level set* of a continuously differentiable function $h : \mathcal{D} \subseteq \mathbb{R}^n \rightarrow \mathbb{R}$ yielding,

$$\mathcal{C} = \{x \in \mathcal{D} \subset \mathbb{R}^n : h(x) \geq 0\} \quad (6)$$

$$\partial\mathcal{C} = \{x \in \mathcal{D} \subset \mathbb{R}^n : h(x) = 0\} \quad (7)$$

$$\text{Int}(\mathcal{C}) = \{x \in \mathcal{D} \subset \mathbb{R}^n : h(x) > 0\} \quad (8)$$

It is assumed that $\text{Int}(\mathcal{C})$ is non-empty and \mathcal{C} has no isolated points, i.e. $\text{Int}(\mathcal{C}) \neq \emptyset$ and $\overline{\text{Int}(\mathcal{C})} = \mathcal{C}$. The system is safe w.r.t. the control law $u = k(x)$ if $\forall x(0) \in \mathcal{C} \implies x(t) \in \mathcal{C} \quad \forall t \geq 0$. We can mathematically verify if the controller $k(x)$ is safeguarding or not by using Control Barrier Functions (CBFs), which is defined next.

Definition 1 (Control barrier function (CBF)): Given the set \mathcal{C} defined by (6)-(8), with $\frac{\partial h}{\partial x}(x) \neq 0 \quad \forall x \in \partial\mathcal{C}$, the function h is called the control barrier function (CBF) defined on the set \mathcal{D} , if there exists an extended class \mathcal{K} function κ such that for all $x \in \mathcal{D}$:

$$\sup_{u \in \mathbb{U}} \left[\underbrace{\mathcal{L}_f h(x) + \mathcal{L}_g h(x)u + \kappa(h(x))}_{\dot{h}(x,u)} \right] \geq 0 \quad (9)$$

where $\mathcal{L}_f h(x) = \frac{\partial h}{\partial x} f(x)$ and $\mathcal{L}_g h(x) = \frac{\partial h}{\partial x} g(x)$ are the Lie derivatives.

Given this definition of a CBF, we know from [6] and [23] that any Lipschitz continuous control law $k(x)$ satisfying the inequality: $\dot{h} + \kappa(h) \geq 0$ ensures safety of \mathcal{C} if $x(0) \in \mathcal{C}$, and asymptotic convergence to \mathcal{C} if $x(0)$ is outside of \mathcal{C} . It is worth mentioning that CBFs can be also defined just on \mathcal{C} , wherein we ensure only safety. This will be useful for the bicycle model (4), which is described later on.

C. Controller synthesis for real-time safety

Having described the CBF and its associated formal results, we now discuss its Quadratic Programming (QP) formulation. CBFs are typically regarded as *safety filters* which take the desired input (reference controller input) $u_{ref}(x, t)$ and modify this input in a minimal way:

$$\begin{aligned} u^*(x, t) = \min_{u \in \mathbb{U} \subseteq \mathbb{R}^m} & \|u - u_{ref}(x, t)\|^2 \\ \text{s.t. } & \mathcal{L}_f h(x) + \mathcal{L}_g h(x)u + \kappa(h(x)) \geq 0 \end{aligned} \quad (10)$$

This is called the Control Barrier Function based Quadratic Program (CBF-QP). If $\mathbb{U} = \mathbb{R}^m$, then the QP is feasible, and the explicit solution is given by

$$u^*(x, t) = u_{ref}(x, t) + u_{safe}(x, t)$$

where $u_{safe}(x, t)$ is given by

$$u_{safe}(x, t) = \begin{cases} 0 & \text{for } \psi(x, t) \geq 0 \\ -\frac{\mathcal{L}_g h(x)^T \psi(x, t)}{\mathcal{L}_g h(x) \mathcal{L}_g h(x)^T} & \text{for } \psi(x, t) < 0 \end{cases} \quad (11)$$

where $\psi(x, t) := \dot{h}(x, u_{ref}(x, t)) + \kappa(h(x))$. The sign change of ψ yields a switching type of a control law.

D. Classical CBFs and moving obstacle avoidance

Having introduced CBFs, we now explore collision avoidance in unmanned ground vehicles (UGVs). In particular, we discuss the problems associated with the classical CBF-QPs, especially with the velocity obstacles. We also summarize and compare with C3BFs in Table I.

1) *Ellipse-CBF Candidate - Unicycle*: Consider the following CBF candidate:

$$h(x, t) = \left(\frac{c_x(t) - x_p}{c_1} \right)^2 + \left(\frac{c_y(t) - y_p}{c_2} \right)^2 - 1, \quad (12)$$

which approximates an obstacle with an ellipse with center $(c_x(t), c_y(t))$ and axis lengths c_1, c_2 . We assume that $c_x(t), c_y(t)$ are differentiable and their derivatives are piecewise constants. Since h in (12) is dependent on time (e.g. moving obstacles), the resulting set \mathcal{C} is also dependent on time. To analyze this class of sets, time dependent versions of CBFs can be used [24]. Alternatively, we can reformulate our problem to treat the obstacle position c_x, c_y as states, with their derivatives being constants. This will allow us to continue using the classical CBF given by Definition 1 including its properties on safety. The derivative of (12) is

$$\frac{2(c_x - x)(\dot{c}_x - v \cos \theta)}{c_1^2} + \frac{2(c_y - y)(\dot{c}_y - v \sin \theta)}{c_2^2}, \quad (13)$$

which has no dependency on the inputs a, α . Hence, h will not be a valid CBF for the acceleration based model (1). However, for static obstacles, if we choose to use the velocity model (with v, ω as inputs instead of a, α), then h will certainly be a valid CBF, but the vehicle will have limited control capability i.e., it loses steering ω .

2) *Ellipse-CBF Candidate - Bicycle*: For the bicycle model, the derivative of h (12) yields

$$\begin{aligned} \dot{h} = & 2(c_x - x_p)(\dot{c}_x - v \cos \theta + v(\sin \theta)\beta)/c_1^2 \\ & + 2(c_y - y_p)(\dot{c}_y - v \sin \theta - v(\cos \theta)\beta)/c_2^2, \end{aligned} \quad (14)$$

which only has β as the input. Furthermore, the derivatives \dot{c}_x, \dot{c}_y are free variables i.e., the obstacle velocities can be selected in such a way that the constraint $\dot{h}(x, u) + \kappa(h(x)) < 0$, whenever $\mathcal{L}_g h = 0$. This implies that h is not a valid CBF for moving obstacles.

It is worth mentioning that for the acceleration controlled unicycle models (1), we can use another class of CBFs introduced specifically for constraints with higher relative degree [25], [26], [27]. However, our goal in this paper is to develop a generic CBF formulation that provide safety guarantees in both the unicycle and bicycle models. We propose this next.

CBFs	Vehicle Models	Static Obstacle (c_x, c_y)	Moving Obstacle $(c_x(t), c_y(t))^\dagger$
Ellipse CBF	Acceleration controlled unicycle (1)	Not a valid CBF	Not a valid CBF
Ellipse CBF	Bicycle (4)	Valid CBF, No acceleration	Not a valid CBF
C3BF	Acceleration controlled unicycle (1)	Valid CBF in \mathcal{D}	Valid CBF in \mathcal{D}
C3BF	Bicycle (4)	Valid CBF in \mathcal{C}	Valid CBF in \mathcal{C}

$\dagger (c_x(t), c_y(t))$ are continuous (or atleast piece-wise continuous) functions of time

TABLE I: Comparison between the CBFs: Ellipse CBF (12), and the proposed C3BF for different vehicle models.

III. COLLISION CONE CBF (C3BF)

Having described the short-comings of existing approaches for collision avoidance, we will now describe the proposed method i.e., the collision cone CBFs (C3BFs). A collision cone, defined for a pair of objects, is a set which can be used to predict the possibility of collision between the two objects based on the direction of their relative velocity. Collision cone of an object pair represents the directions, which if traversed by either objects, will result in a collision between the two. We will treat the obstacles as ellipses with the vehicle reduced to a point; therefore, throughout the rest of the paper, the term collision cone will refer to this case with the ego-vehicle's center being the point of reference.

Consider an ego-vehicle defined by the system (5) and a moving obstacle (pedestrian, another vehicle, etc.). This is shown pictorially in Fig. 3. We define the velocity and positions of the obstacle w.r.t. the ego vehicle. We *over-approximated* the obstacle to be an ellipse and draw two tangents from the vehicle's centre to a conservative circle encompassing the ellipse, taking into account the ego-vehicle's dimensions ($r = \max(c_1, c_2) + \frac{\text{Width}_{\text{vehicle}}}{2}$). For a collision to happen, the relative velocity of the obstacle must be pointing towards the vehicle. Hence, the relative velocity vector must not be pointing into the pink shaded region EHI in Fig. 3, which is a cone. Let \mathcal{C} be this set of safe directions for this relative velocity vector. If there exists a function $h : \mathcal{D} \subseteq \mathbb{R}^n \rightarrow \mathbb{R}$ satisfying *Definition: 1* on \mathcal{C} , then we know that a Lipschitz continuous control law obtained from the resulting QP (10) for the system ensures that the vehicle won't collide with the obstacle even if the reference u_{ref} tries to direct them towards a collision course. This novel approach of avoiding the pink cone region gives rise to **Collision Cone Control Barrier Functions (C3BFs)**.

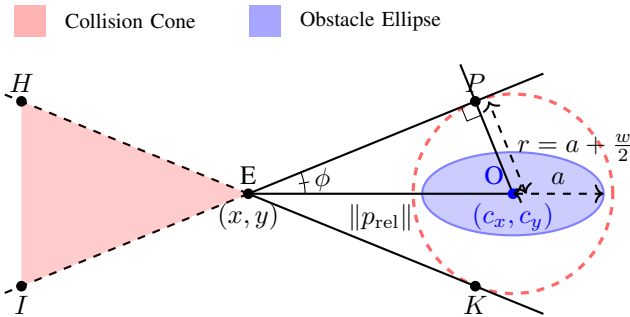


Fig. 3: Construction of collision cone for an elliptical obstacle considering the ego-vehicle's dimensions (width: w).

A. Application to systems

1) Acceleration controlled unicycle model: We first obtain the relative position vector between the body center of the unicycle and the center of the obstacle. Therefore, we have

$$p_{\text{rel}} := \begin{bmatrix} c_x - (x_p + l \cos(\theta)) \\ c_y - (y_p + l \sin(\theta)) \end{bmatrix} \quad (15)$$

Here l is the distance of the body center from the differential drive axis (see Fig. 2). We obtain its velocity as

$$v_{\text{rel}} := \begin{bmatrix} \dot{c}_x - (v \cos(\theta) - l \sin(\theta) * \omega) \\ \dot{c}_y - (v \sin(\theta) + l \cos(\theta) * \omega) \end{bmatrix}. \quad (16)$$

We propose the following CBF candidate:

$$h(x, t) = \langle p_{\text{rel}}, v_{\text{rel}} \rangle + \|p_{\text{rel}}\| \|v_{\text{rel}}\| \cos \phi \quad (17)$$

where, ϕ is the half angle of the cone, the expression of $\cos \phi$ is given by $\frac{\sqrt{\|p_{\text{rel}}\|^2 - r^2}}{\|p_{\text{rel}}\|}$ (see Fig. 3). The constraint simply ensures that the angle between $p_{\text{rel}}, v_{\text{rel}}$ is less than $180^\circ - \phi$. We have the following first result of the paper:

Theorem 1: Given the acceleration controlled unicycle model (1), the proposed CBF candidate (17) with $p_{\text{rel}}, v_{\text{rel}}$ defined by (15), (16) is a valid CBF defined for the set \mathcal{D} .

Proof: Taking the derivative of (17) yields

$$\begin{aligned} \dot{h} &= \langle \dot{p}_{\text{rel}}, v_{\text{rel}} \rangle + \langle p_{\text{rel}}, \dot{v}_{\text{rel}} \rangle \\ &+ \langle v_{\text{rel}}, \dot{v}_{\text{rel}} \rangle \frac{\sqrt{\|p_{\text{rel}}\|^2 - r^2}}{\|v_{\text{rel}}\|} \\ &+ \langle p_{\text{rel}}, \dot{p}_{\text{rel}} \rangle \frac{\|v_{\text{rel}}\|}{\sqrt{\|p_{\text{rel}}\|^2 - r^2}}. \end{aligned} \quad (18)$$

Further $\dot{p}_{\text{rel}} = v_{\text{rel}}$ and

$$\dot{v}_{\text{rel}} = \begin{bmatrix} -a \cos \theta + v(\sin \theta) \omega + l(\cos \theta) \omega^2 + l(\sin \theta) \alpha \\ -a \sin \theta - v(\cos \theta) \omega + l(\sin \theta) \omega^2 - l(\cos \theta) \alpha \end{bmatrix}.$$

Given \dot{v}_{rel} and \dot{h} , we have the following expression for $\mathcal{L}_g h$:

$$\mathcal{L}_g h = \begin{bmatrix} \langle p_{\text{rel}} + v_{\text{rel}} \frac{\sqrt{\|p_{\text{rel}}\|^2 - r^2}}{\|v_{\text{rel}}\|}, \begin{bmatrix} -\cos \theta \\ -\sin \theta \end{bmatrix} \rangle \\ \langle p_{\text{rel}} + v_{\text{rel}} \frac{\sqrt{\|v_{\text{rel}}\|^2 - r^2}}{\|v_{\text{rel}}\|}, \begin{bmatrix} l \sin \theta \\ -l \cos \theta \end{bmatrix} \rangle \end{bmatrix}^T, \quad (19)$$

It can be verified that for $\mathcal{L}_g h$ to be zero, we can have the following scenarios:

- $p_{\text{rel}} + v_{\text{rel}} \frac{\sqrt{\|p_{\text{rel}}\|^2 - r^2}}{\|v_{\text{rel}}\|} = 0$, which is not possible. Firstly, $p_{\text{rel}} = 0$ indicates that the vehicle is already inside the obstacle. Secondly, if the above equation were to be true for a non-zero p_{rel} , then $v_{\text{rel}}/\|v_{\text{rel}}\| = -p_{\text{rel}}/\sqrt{\|p_{\text{rel}}\|^2 - r^2}$. This is also not possible as the magnitude of LHS is 1, while that of RHS is > 1 .

- $p_{\text{rel}} + v_{\text{rel}} \frac{\sqrt{\|v_{\text{rel}}\|^2 - r^2}}{\|v_{\text{rel}}\|}$ is perpendicular to both $\begin{bmatrix} -\cos \theta \\ -\sin \theta \end{bmatrix}$ and $\begin{bmatrix} l \sin \theta \\ -l \cos \theta \end{bmatrix}$, which is also not possible.

This implies that $\mathcal{L}_g h$ is always a non-zero matrix, implying that h is a valid CBF. ■

Remark 2: Since $\mathcal{L}_g h \neq 0$, we can infer from [28, Theorem 8] that the resulting QP given by (11) is Lipschitz continuous. Hence, we can construct CBF-QPs with the proposed CBF (17) for the unicycle model and guarantee collision avoidance. In addition, if $h(x(0)) < 0$, then we can construct a class \mathcal{K} function κ in such a way that the magnitude of h exponentially decreases over time, thereby minimizing the violation. We will demonstrate these scenarios in Section IV.

2) *Acceleration controlled Bicycle model:* For the approximated bicycle model (4), we define the following:

$$p_{\text{rel}} := [c_x - x_p \quad c_y - y_p]^T \quad (20)$$

$$v_{\text{rel}} := [\dot{c}_x - v \cos \theta \quad \dot{c}_y - v \sin \theta]^T, \quad (21)$$

Here v_{rel} is NOT equal to the relative velocity \dot{p}_{rel} . However, for small β , we can assume that v_{rel} is the difference between obstacle velocity and the velocity component along the length of the vehicle $v \cos \beta \approx v$. In other words, the goal is to ensure that this approximated velocity v_{rel} is pointing away from the cone. This is an acceptable approximation as β is small and the obstacle radius chosen was conservative (see Fig. 3). We have the following result:

Theorem 2: Given the bicycle model (4), the proposed candidate CBF (17) with $p_{\text{rel}}, v_{\text{rel}}$ defined by (20), (21) is a valid CBF defined for the set \mathcal{C} .

Proof: We need to show that $\mathcal{L}_g h = 0 \implies \dot{h} + \kappa(h) \geq 0$. The derivative of h (17) yields (18). Further using (4): $\dot{p}_{\text{rel}} = v_{\text{rel}} + \beta [v \sin \theta, -v \cos \theta]^T$ and

$$\dot{v}_{\text{rel}} = \begin{bmatrix} -\cos \theta & v \sin \theta \\ -\sin \theta & -v \cos \theta \end{bmatrix} \begin{bmatrix} a \\ \frac{v}{l_r} \beta \end{bmatrix}. \quad (22)$$

When $\mathcal{L}_g h = 0$, we have

$$\dot{h} + \kappa(h) = \langle v_{\text{rel}}, v_{\text{rel}} \rangle + \frac{\langle p_{\text{rel}}, v_{\text{rel}} \rangle \|v_{\text{rel}}\|}{\sqrt{\|p_{\text{rel}}\|^2 - r^2}} + \kappa(h).$$

Rewriting the above equation yields

$$\frac{\|v_{\text{rel}}\|}{\sqrt{\|p_{\text{rel}}\|^2 - r^2}} \left(h + \frac{\sqrt{\|p_{\text{rel}}\|^2 - r^2}}{\|v_{\text{rel}}\|} \kappa(h) \right). \quad (23)$$

Since $\sqrt{\|p_{\text{rel}}\|^2 - r^2}$ and $\|v_{\text{rel}}\|$ are positive quantities, the entire quantity above is ≥ 0 for all $x \in \mathcal{C}$. This completes the proof. ■

Remark 3: Theorem 2 is different from Theorem 1 as the CBF inequality is satisfied in the set \mathcal{C} and not in \mathcal{D} . In other words, forward invariance of \mathcal{C} can be guaranteed, but not asymptotic convergence of \mathcal{C} . However modifications of the control formulation is possible to extend the result for \mathcal{D} , which will a subject of future work.

IV. RESULTS AND DISCUSSIONS

In this section, we provide the simulation and experimental results to validate the proposed C3BF-QP. We will first demonstrate the results in python simulation, and then demonstrate on the Copernicus UGV (modeled as a unicycle), and on the autonomous car in CARLA simulator (modeled as a bicycle).

A. Acceleration Controlled Unicycle Model

In both simulation and experiments we have considered the reference control inputs as a simple P-controller formulated as follows:

$$u_{\text{ref}}(x, t) = \begin{bmatrix} a_{\text{ref}}(x, t) \\ \alpha_{\text{ref}}(x, t) \end{bmatrix} = \begin{bmatrix} k_1 * (v_{\text{des}} - v) \\ -k_2 * \omega \end{bmatrix} \quad (24)$$

where k_1, k_2 are constant gains, $v_{\text{des}} \leq v_{\text{max}}$ is the target velocity of vehicle. We chose constant target velocities for verifying the C3BF-QP. For the class \mathcal{K} function in the CBF inequality, we chose $\kappa(h) = \gamma h$, where $\gamma = 1$. However, the reference controller can be replaced by any trajectory tracking controller like the Stanley controller [29]. A virtual perception boundary was incorporated considering the maximum range for the perception sensors. As soon as an obstacle is detected within the perception boundary, the C3BF-QP is activated with u_{ref} given by (24). The QP yields the optimal accelerations, which are then applied to the robot.

1) *Python Simulation:* We consider different scenarios with different poses and velocities of both the vehicle and the obstacle. Different scenarios include static obstacle resulting in a) turning; b) braking and moving obstacle resulting in c) reversing; d) overtaking, as shown in Fig. 4. The corresponding evolution of CBF value (h) as a function of time is shown in Fig. 5. We can observe that even if $h < 0$ at $t = 0$ (Fig. 5(b),(c)), the magnitude is exponentially decreasing.

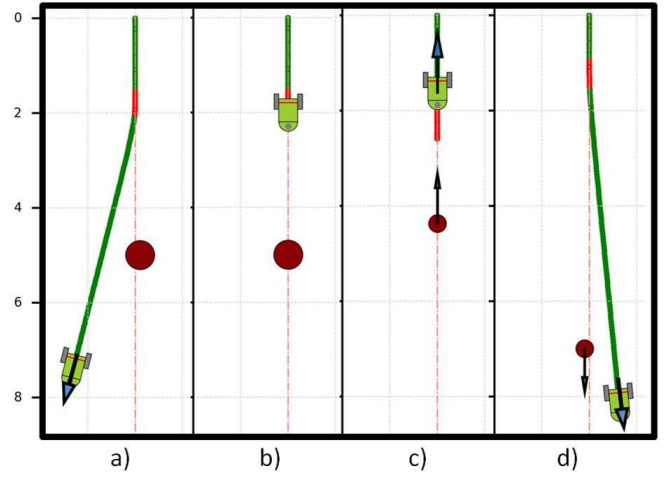


Fig. 4: Different vehicle behaviours with static (a,b) & moving (c,d) obstacle. a) turning; b) braking; c) reversing; d) overtaking.

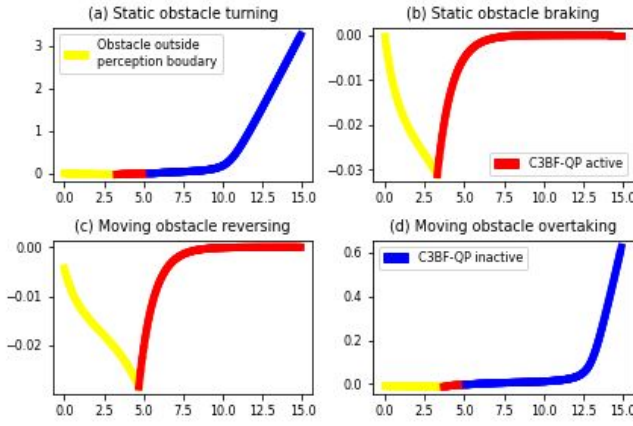


Fig. 5: CBF value (h) (Y-axis) varying with time (X-axis). C3BF-QP active means $u_{safe} \neq 0$ (Red) and C3BF-QP inactive means $u_{safe} = 0$ (Blue).

2) *Hardware Experiments*: Corresponding to the cases tested in Python simulation, experiments were performed on the Botsync's Copernicus UGV. It is a differential drive (4X4) robot with dimensions 860 x 760 x 590 mm. Apart from its internal wheel encoders, external sensors like Ouster OS1-128 Lidar and Xsens IMU MCI-670G sensor were used for localization and minimizing the odometric error through LIO-SAM algorithm [30]. Zed-2 Stereo camera was used to detect the obstacles through masking and image segmentation techniques and to get their positions using the depth information.

Our C3BF algorithm combined with the perception stack was first simulated in the Gazebo environment and then tested on the actual robot. Depending on the different initial poses of Copernicus, and different positions, velocities of obstacles, we observed braking, turning, reversal and overtaking behaviours. These behaviours were similar to the results obtained from python simulations. We also experimented various scenarios with multiple stationary obstacles. Even though the behaviours are sensitive to the initial conditions of the robot and obstacle, collision is avoided in all the cases. All the results are shown in the supplement video¹.

B. Acceleration Controlled Bicycle Model

We have extended and validated our C3BF algorithm for the bicycle model (4) which is a good approximation of actual car dynamics under the assumption of small lateral acceleration ($\leq 0.5\mu g$, μ is the friction co-efficient) [9] [22]. The linear acceleration reference control a_{ref} was obtained from a P-controller tracking the desired velocity, and the steering reference β_{ref} was obtained from the Stanley controller [29]. The Stanley controller is fed an explicit reference spline trajectory for tracking, with obstacle on it. The reference controllers were integrated with the C3BF-QP, and applied to the robot simulated in Python (Fig. 6) and CARLA simulator (Fig. 1).

1) *Python Simulations*: Fig. 6 shows the trajectory setup along with an obstacle placed towards the end. The ego

vehicle tracks the reference spline trajectory (red) and the reflection of collision cone is shown by the pink region. The C3BF algorithm preemptively prevents the relative velocity vector from falling into the unsafe set, thus avoiding obstacle by circum-navigating. It can be verified from Fig. (6b) that the slip angle β remains small which is in line with the assumption used (4).

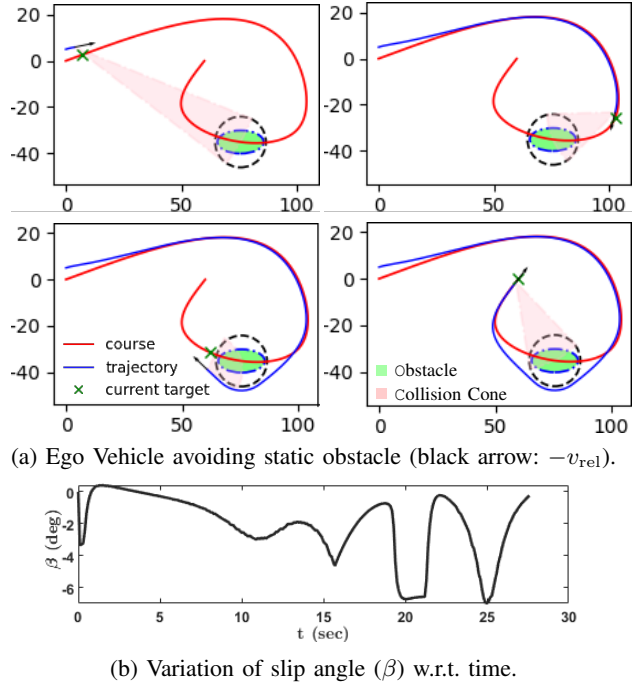


Fig. 6: Graphical illustration of C3BF on bicycle model (4).

2) *CARLA Simulations*: With the small β approximation and using the formulation from section III-A.2, numerical simulations (using *CVXOPT* library) were performed on virtual car model on CARLA simulator [31] to demonstrate the efficacy of C3BF in collision avoidance in real-world like environments. To accommodate the range of perception sensors on real self-driving cars, a virtual perception boundary was used. Information about the obstacle is programmatically retrieved from the CARLA server. The resulting simulations can be viewed in the supplement video¹.

V. CONCLUSIONS

We presented a novel CBF formulation for collision avoidance with moving obstacles, by using the concept of collision cones. Existing works in literature were not able to circumnavigate / brake in the presence of obstacles with non-zero velocity values. The proposed QP formulation (C3BF-QP) allows the vehicle to safely maneuver under different scenarios presented in the paper. As a part of future work, focus will be more on autonomous cars with obstacles like pedestrians, incoming cars and other types of moving objects. The possibility of C3BF application to drones can also be explored.

¹ <https://youtu.be/0P6ycij5uiw>

REFERENCES

- [1] S. Yu, M. Hirche, Y. Huang, H. Chen, and F. Allgöwer, "Model predictive control for autonomous ground vehicles: a review," *Autonomous Intelligent Systems*, vol. 1, 12 2021.
- [2] I. Kolmanovsky, E. Garone, and S. Di Cairano, "Reference and command governors: A tutorial on their theory and automotive applications," in *2014 American Control Conference*, 2014, pp. 226–241.
- [3] S. Bansal, M. Chen, S. Herbert, and C. J. Tomlin, "Hamilton-jacobi reachability: A brief overview and recent advances," in *2017 IEEE 56th Annual Conference on Decision and Control (CDC)*, 2017, pp. 2242–2253.
- [4] Z. Li, "Comparison between safety methods control barrier function vs. reachability analysis," 2021. [Online]. Available: <https://arxiv.org/abs/2106.13176>
- [5] A. W. Singletary, K. Klingebiel, J. R. Bourne, N. A. Browning, P. T. Tokumaru, and A. D. Ames, "Comparative analysis of control barrier functions and artificial potential fields for obstacle avoidance," *2021 IEEE/RSJ International Conference on Intelligent Robots and Systems (IROS)*, pp. 8129–8136, 2021.
- [6] A. D. Ames, X. Xu, J. W. Grizzle, and P. Tabuada, "Control barrier function based quadratic programs for safety critical systems," *IEEE Transactions on Automatic Control*, vol. 62, no. 8, pp. 3861–3876, aug 2017. [Online]. Available: <https://doi.org/10.1109%2Ftac.2016.2638961>
- [7] A. Manjunath and Q. Nguyen, "Safe and robust motion planning for dynamic robotics via control barrier functions," in *2021 60th IEEE Conference on Decision and Control (CDC)*, 2021, pp. 2122–2128.
- [8] A. D. Ames, J. W. Grizzle, and P. Tabuada, "Control barrier function based quadratic programs with application to adaptive cruise control," in *53rd IEEE Conference on Decision and Control*, 2014, pp. 6271–6278.
- [9] S. He, J. Zeng, B. Zhang, and K. Sreenath, "Rule-based safety-critical control design using control barrier functions with application to autonomous lane change," 2021. [Online]. Available: <https://arxiv.org/abs/2103.12382>
- [10] Y. Chen, H. Peng, and J. Grizzle, "Obstacle avoidance for low-speed autonomous vehicles with barrier function," *IEEE Transactions on Control Systems Technology*, vol. 26, no. 1, pp. 194–206, 2018.
- [11] T. D. Son and Q. Nguyen, "Safety-critical control for non-affine nonlinear systems with application on autonomous vehicle," in *2019 IEEE 58th Conference on Decision and Control (CDC)*, 2019, pp. 7623–7628.
- [12] Y. Chen, A. Singletary, and A. D. Ames, "Guaranteed obstacle avoidance for multi-robot operations with limited actuation: A control barrier function approach," *IEEE Control Systems Letters*, vol. 5, no. 1, pp. 127–132, 2021.
- [13] M. Abduljabbar, N. Meskin, and C. G. Cassandras, "Control barrier function-based lateral control of autonomous vehicle for roundabout crossing," in *2021 IEEE International Intelligent Transportation Systems Conference (ITSC)*, 2021, pp. 859–864.
- [14] A. Chakravarthy and D. Ghose, "Obstacle avoidance in a dynamic environment: a collision cone approach," *IEEE Transactions on Systems, Man, and Cybernetics - Part A: Systems and Humans*, vol. 28, no. 5, pp. 562–574, 1998.
- [15] P. Fiorini and Z. Shiller, "Motion planning in dynamic environments using the relative velocity paradigm," in *[1993] Proceedings IEEE International Conference on Robotics and Automation*, 1993, pp. 560–565 vol.1.
- [16] ———, "Motion planning in dynamic environments using velocity obstacles," *The International Journal of Robotics Research*, vol. 17, no. 7, pp. 760–772, 1998. [Online]. Available: <https://doi.org/10.1177/027836499801700706>
- [17] A. Chakravarthy and D. Ghose, "Generalization of the collision cone approach for motion safety in 3-d environments," *Autonomous Robots*, vol. 32, no. 3, pp. 243–266, Apr 2012. [Online]. Available: <https://doi.org/10.1007/s10514-011-9270-z>
- [18] D. Bhattacharjee, A. Chakravarthy, and K. Subbarao, "Nonlinear model predictive control and collision-cone-based missile guidance algorithm," *Journal of Guidance, Control, and Dynamics*, vol. 44, no. 8, pp. 1481–1497, 2021. [Online]. Available: <https://doi.org/10.2514/1.G005879>
- [19] J. Goss, R. Rajvanshi, and K. Subbarao, *Aircraft Conflict Detection and Resolution Using Mixed Geometric And Collision Cone Approaches*. AIAA Guidance, Navigation, and Control Conference and Exhibit, 2004, ch. 0, p. 0. [Online]. Available: <https://arc.aiaa.org/doi/abs/10.2514/6.2004-4879>
- [20] M. Babu, Y. Oza, A. K. Singh, K. M. Krishna, and S. Medasani, "Model predictive control for autonomous driving based on time scaled collision cone," in *2018 European Control Conference (ECC)*. IEEE, 2018, pp. 641–648.
- [21] R. Rajamani, *Vehicle dynamics and control*, 2nd ed., ser. Mechanical Engineering Series. New York, NY: Springer, Mar. 2014.
- [22] P. Polack, F. Altché, B. d'Andréa Novel, and A. de La Fortelle, "The kinematic bicycle model: A consistent model for planning feasible trajectories for autonomous vehicles?" in *2017 IEEE Intelligent Vehicles Symposium (IV)*, 2017, pp. 812–818.
- [23] A. D. Ames, S. Coogan, M. Egerstedt, G. Notomista, K. Sreenath, and P. Tabuada, "Control barrier functions: Theory and applications," in *2019 18th European Control Conference (ECC)*, 2019, pp. 3420–3431.
- [24] M. Igarashi, I. Tezuka, and H. Nakamura, "Time-varying control barrier function and its application to environment-adaptive human assist control," *IFAC-PapersOnLine*, vol. 52, no. 16, pp. 735–740, 2019, 11th IFAC Symposium on Nonlinear Control Systems NOLCOS 2019. [Online]. Available: <https://www.sciencedirect.com/science/article/pii/S2405896319318804>
- [25] Q. Nguyen and K. Sreenath, "Exponential control barrier functions for enforcing high relative-degree safety-critical constraints," in *2016 American Control Conference (ACC)*, 2016, pp. 322–328.
- [26] W. Xiao and C. Belta, "Control barrier functions for systems with high relative degree," 2019. [Online]. Available: <https://arxiv.org/abs/1903.04706>
- [27] X. Tan, W. S. Cortez, and D. V. Dimarogonas, "High-order barrier functions: Robustness, safety, and performance-critical control," *IEEE Transactions on Automatic Control*, vol. 67, no. 6, pp. 3021–3028, 2022.
- [28] X. Xu, P. Tabuada, J. W. Grizzle, and A. D. Ames, "Robustness of control barrier functions for safety critical control." *IFAC-PapersOnLine*, vol. 48, no. 27, pp. 54–61, 2015, analysis and Design of Hybrid Systems ADHS. [Online]. Available: <https://www.sciencedirect.com/science/article/pii/S2405896315024106>
- [29] G. M. Hoffmann, C. J. Tomlin, M. Montemerlo, and S. Thrun, "Autonomous automobile trajectory tracking for off-road driving: Controller design, experimental validation and racing," in *2007 American Control Conference*, 2007, pp. 2296–2301.
- [30] T. Shan, B. Englot, D. Meyers, W. Wang, C. Ratti, and R. Daniela, "Lio-sam: Tightly-coupled lidar inertial odometry via smoothing and mapping," in *IEEE/RSJ International Conference on Intelligent Robots and Systems (IROS)*. IEEE, 2020, pp. 5135–5142.
- [31] A. Dosovitskiy, G. Ros, F. Codevilla, A. Lopez, and V. Koltun, "CARLA: An open urban driving simulator," in *Proceedings of the 1st Annual Conference on Robot Learning*, 2017, pp. 1–16.